J|A|C|S
ARTICLES
Published on Web 01/05/2002

Electrochemical Characterization of Polyacetylene Ionomers and Polyelectrolyte-Mediated Electrochemistry toward Interfaces between Dissimilarly Doped Conjugated Polymers

Mark C. Lonergan,* Calvin H. Cheng, Brandi L. Langsdorf, and X. Zhou

Contribution from the Department of Chemistry and The Materials Science Institute, University of Oregon, Eugene, Oregon 97403

Received July 26, 2001. Revised Manuscript Received November 7, 2001

Abstract: The electrochemical characterization of thin films of the ionically functionalized polyacetylene analogues poly(tetramethylammonium 2-cyclooctatetraenylethanesulfonate) (P_A) and poly[(2-cyclooctatetraenylethyl)trimethylammonium trifluoromethanesulfonate] (P_C) is reported along with an electrochemical approach to the fabrication of interfaces between dissimilarly doped conjugated polymers. Such interfaces are of interest because of the central role analogous interfaces based on silicon play in conventional microelectronics. The cationically functionalized P_C can be both oxidatively (p-type) and reductively (n-type) doped to a conductive state, whereas the anionically functionalized P_A can only be p-type doped. The voltammetry of P_C displays relatively sharp waves with minimal history or relaxation effects. In contrast, the voltammetry of P_A exhibits broader doping waves and a dependence on electrochemical history. The apparent formal potentials reported in 0.075 M Me_4NBF_4/CH_3CN were −1.04 V versus SCE for the n-doping of P_C and 0.40 and 0.30 V versus SCE for the p-doping of P_C and P_A, respectively. These values depend on electrolyte concentration consistent with a Donnan potential due to the selective partitioning of ions between the electrolyte and polymer. Electrochemical quartz crystal microbalance data demonstrate that the p-type doping of P_A and the n-type doping of P_C proceed with the loss of ions from the polymer film and the formation of the internally compensated state. Voltammetry in tetrabutylammonium poly(styrenesulfonate)/CH_3CN supporting electrolyte is also reported. It is demonstrated how a polyanion supporting electrolyte in concert with a conjugated ionomer can be used to control redox chemistry by governing the sign of ions available for charge compensation. In particular, we demonstrate the self-limiting oxidation of P_A to inhibit deleterious overoxidation and prepare the precisely internally compensated state; the selective oxidation of P_A over P_C, despite their similar apparent formal potentials; and the inhibition of the reoxidation of the n-doped form of P_C. The use of such polyelectrolyte-mediated electrochemistry in the fabrication of interfaces between dissimilarly doped conjugated polymers is discussed.

Introduction

Central to conventional silicon microelectronics are interfaces between regions of silicon with different doping types (n vs p) or densities.[1] Analogous interfaces based on conjugated polymers are of interest as components of electronic devices based on organic materials. For instance, the performance of organic light-emitting diodes utilizing a nominally undoped conjugated polymer can be improved by the incorporation of a doped polymer electrode[2] and photovoltaics based on doped | undoped polymer interfaces have been recently reported.[3]

Although thermodynamically unstable, interfaces between dissimilarly doped regions of silicon are kinetically stable due to the immobility of the dopant atoms. In contrast, the dopant ions of conventionally doped conjugated polymers can be mobile. The mobility of dopant ions in conventional conjugated polymers presents a potential problem in the fabrication of interfaces between dissimilarly doped conjugated polymers. Bulk chemical reactions between conjugated polymers of different doping types or densities can occur as the result of the mobility of dopant atoms in conjugated polymers.[4] The rate of such a reaction depends on ion diffusion coefficients, which in turn depends on the ion, polymer structure, and any incorporated solvent or other additive. A simple illustration of the reactivity between regions of conjugated polymers with different doping types is the transient stability of the *p*-type | *i*ntrinsic | *n*-type (*p*-*i*-*n*) structure formed during the operation of electrochemical light-emitting diodes.[5]

In principle, bulk chemical reactions between dissimilarly doped conjugated polymers can be prevented either on a thermodynamic or a kinetic basis. An example of thermody-

(1) Sze, S. M. *Physics of Semiconductor Devices*; Wiley: New York, 1981.
(2) Gross, M.; Muller, D. C.; Nothofer, H.-G.; Scherf, U.; Neher, D.; Brauchle, C.; Meerholz, K. *Nature* **2000**, *405*, 661−665.
(3) Arias, A. C.; Granstrom, M.; Thomas, D. S.; Petritsch, K.; Friend, R. H. *Phys. Rev. B* **1999**, *60*, 1854−1860.
(4) Zhou, Z.; Langsdorf, B. L.; Lonergan, M. C. *Mater. Res. Soc. Symp. Proc.* **2000**, *598*, BB5.7/1−BB5.7/6 (Electrical, Optical, and Magnetic Properties of Organic Solid-State Materials V).
(5) Pei, Q.; Yu, G.; Zhang, C.; Yang, Y.; Heeger, A. J. *Science* **1995**, *269*, 1086.

10.1021/ja016715z CCC: $22.00

Chart 1

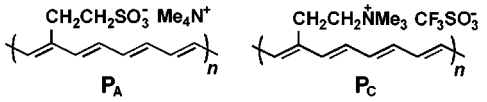

namic control comes from bilayer structures[6,7] such as that between polypyrrole and poly(3-octylthiophene). Here the separation in reduction potential ($E°$) for p-doping these polymers allows for polypyrrole to be selectively oxidized in the bilayer while leaving polythiophene undoped.[7] In relation to electronic devices, such interfaces would correspond to heterojunctions based on different inorganic semiconductors. "Homojunctions" based on a single polymer backbone would not be possible with such an approach, nor would interfaces between n- and p-type materials, which are generally expected to be unstable on a thermodynamic basis.

Kinetic control over interfacial reactivity can be achieved by controlling ion diffusion. A straightforward way this can be achieved is through the use of internally compensated conjugated polymers in which the dopant ions balancing the charge injected into the polymer backbone are covalently bound to the polymer and hence exhibit very low diffusion coefficients.[4] The long-term stability of interfaces based on such internally compensated polymers is ultimately limited by the time scale for polymer, and hence counterion, diffusion. Such kinetic stability is analogous to that for silicon homojunctions where the diffusion coefficients for dopant atoms sets the relevant time scale. Restricting the mobility of dopant ions in conjugated polymers is also essential in controlling the spatial distribution of charges under applied bias.

To explore the possibility of kinetically controlling bulk chemical reactions between dissimilarly doped conjugated polymers, we have been studying the conjugated ionomers, poly(tetramethylammonium 2-cyclooctatetraenylethanesulfonate) (P_A) and poly[(2-cyclooctatetraenylethyl)trimethylammonium trifluoromethanesulfonate] (P_C) (see Chart 1) in their predominately trans form.[8,9] These materials are of interest herein because they provide for the production of both internally compensated n-type and p-type forms and the exploration of conjugated polymer "homojunctions".

In this paper, we present the voltammetric characterization of films of P_A and P_C in conventional small ion electrolytes, such as tetramethylammonium tetrafluoroborate (Me_4NBF_4), and in a polyanion electrolyte tetrabutylammonium poly(styrenesulfonate) (Bu_4NPSS). The small ion electrolyte studies are essential for understanding the fundamental redox behavior of these polymers. Investigation of the voltammetry of P_A and P_C in the presence of the polyanion electrolyte Bu_4NPSS aids the development of useful tools for the fabrication of interfaces between dissimilarly doped conjugated polymers based on the internally compensated form.

The use of polyelectrolytes in studying the electrochemistry of conjugated polymers is certainly not a new idea. An important driving force for the synthesis of a wide range of conjugated polymers either blended with polyelectrolytes[10−14] or having covalently bound ionic substituents[15−23] has been to control the ion exchange properties of these polymers upon doping. Polyelectrolytes have also been very useful in studying the doping mechanics of conjugated polymers and for fundamental measures of ion transport through polymer films. Pickup and co-workers exploited polyelectrolyte composites and ionically functionalized polypyrroles to study, for instance, the spatial evolution of doping in polymer films, issues of redox versus electronic conduction, and ionic conduction in conjugated polymers.[24,25] Salzer and Elliot used polypyrrole/poly(styrenesulfonate) composites with a poly(styrenesulfonate) supporting electrolyte to study ion transport through polypyrrole films.[26] Earlier work by the Elliot group also demonstrated the use of polycation supporting electrolyte to selectively access one redox wave of a Ru redox polymer.[27] The use of a polycation supporting electrolyte also prevented the formation of redox site concentration gradients to directly probe electronic conductivity. The studies reported herein build on many of these ideas in the context of developing tools for the fabrication of interfaces between dissimilarly doped conjugated polymers where the combination of both anionic and cationic conjugated ionomers and a supporting polyelectrolyte provide a range of new possibilities.

Experimental Section

Materials. Acetonitrile (HPLC grade, Mallinckrodt) was distilled from CaH_2 and then degassed using three freeze−pump−thaw cycles before use. Dimethyl sulfoxide (DMSO, Baker) was distilled from BaO. Anhydrous methanol (Aldrich) was used as received. Me_4NBF_4 (Aldrich) and tetrabutylammonium tetrafluoroborate (Bu_4NBF_4, Aldrich) were recrystallized from ethyl acetate and then dried in vacuo (20 mTorr) for 7 days at 80 °C.

Bu_4NPSS was prepared by ion exchange from sodium poly(styrenesulfonate) (NaPSS, $M_W \approx 50\,000$, Scientific Polymer Products). Dowex 50W-X8 (Baker) was charged by sequential washings with (1) 1 M HCl, (2) H_2O, (3) 40% (w/w) tetrabutylammonium hydroxide (Aldrich), and (4) H_2O. Ion exchange of NaPSS to Bu_4NPSS was then achieved by passage of an aqueous solution down this charged Dowex column. The resulting Bu_4NPSS was dialyzed for several days using Spectra/Por 4 cellulose dialysis membranes and then dried in vacuo (20 mTorr) for 7 days at 80 °C.

The predominately trans forms of poly[$C_8H_7CH_2CH_2SO_3(CH_3)_4N$], P_A, and poly[$C_8H_7CH_2CH_2N(CH_3)_3CF_3SO_3$] were available from a previous study.[9]

(6) Torres, W.; Fox, M. A. *Chem. Mater.* **1990**, *2*, 306−311.
(7) Demoustier-Champagne, S.; Reynolds, J. R.; Pomerantz, M. *Chem. Mater.* **1995**, *7*, 277−283.
(8) Langsdorf, B. L.; Zhou, X.; Adler, D. H.; Lonergan, M. C. *Macromolecules* **1999**, *32*, 2796.
(9) Langsdorf, B. L.; Zhou, X.; Lonergan, M. C. *Macromolecules* **2001**, *34*, 2450−2458.
(10) Shimidzu, T.; Ohtani, A.; Iyoda, T.; Honda, K. *J. Chem. Soc., Chem. Commun.* **1986**, 1415−1417.
(11) Miller, L. L.; Zhou, Q. X. *Macromolecules* **1987**, *20*, 1594−1597.
(12) Hirai, T.; Kuwabata, S.; Yoneyama, H. *J. Electrochem. Soc.* **1988**, *135*, 1132−1137.
(13) Baker, C. K.; Qui, Y. J.; Reynolds, J. R. *J. Phys. Chem.* **1991**, *95*, 4446−4452.
(14) Ren, X.; Pickup, P. G. *J. Phys. Chem.* **1993**, *97*, 5336−5362.
(15) Ikenoue, Y.; Chiang, J.; Patil, A. O.; Wudl, F.; Heeger, A. J. *J. Am. Chem. Soc.* **1988**, *110*, 2983−2985.
(16) Ikenoue, Y.; Uotani, N.; Patil, A. O.; Wudl, F.; Heeger, A. J. *Synth. Met.* **1989**, *30*, 305−319.
(17) Barbero, C.; Kotz, R. *Adv. Mater.* **1994**, *6*, 577−580.
(18) Yue, J.; Epstein, A. J. *J. Am. Chem. Soc.* **1990**, *112*, 2800−2801.
(19) Arroyo-Villan, M. I.; Diaz-Quijada, G. A.; Abdou, M. S. A.; Holdcroft, S. *Macromolecules* **1995**, *28*, 975−984.
(20) Patil, A. O.; Ikenoue, Y.; Wudl, F.; Heeger, A. J. *J. Am. Chem. Soc.* **1987**, *109*, 1858−1859.
(21) Child, A. D.; Reynolds, J. R. *Macromolecules* **1994**, *27*, 1975−1977.
(22) Chen, S.-A.; Hwang, G.-W. *J. Am. Chem. Soc.* **1995**, *117*, 10055−10062.
(23) Ikenoue, Y.; Saida, Y.; Kira, M.; Tomozawa, H.; Yashima, H.; Kobayashi, M. *J. Chem. Soc., Chem. Commun.* **1990**, 1694−1695.
(24) Ren, X.; Pickup, P. G. *J. Phys. Chem.* **1993**, *97*, 3941−3943.
(25) Mao, H.; Pickup, P. G., personal communication, 1990.
(26) Salzer, C. A.; Elliott, C. M. *Anal. Chem.* **1999**, *71*, 3677−3684.
(27) Elliot, C. M.; Redepenning, J. G.; Balk, E. M. *J. Am. Chem. Soc.* **1985**, *107*, 8302−8304.

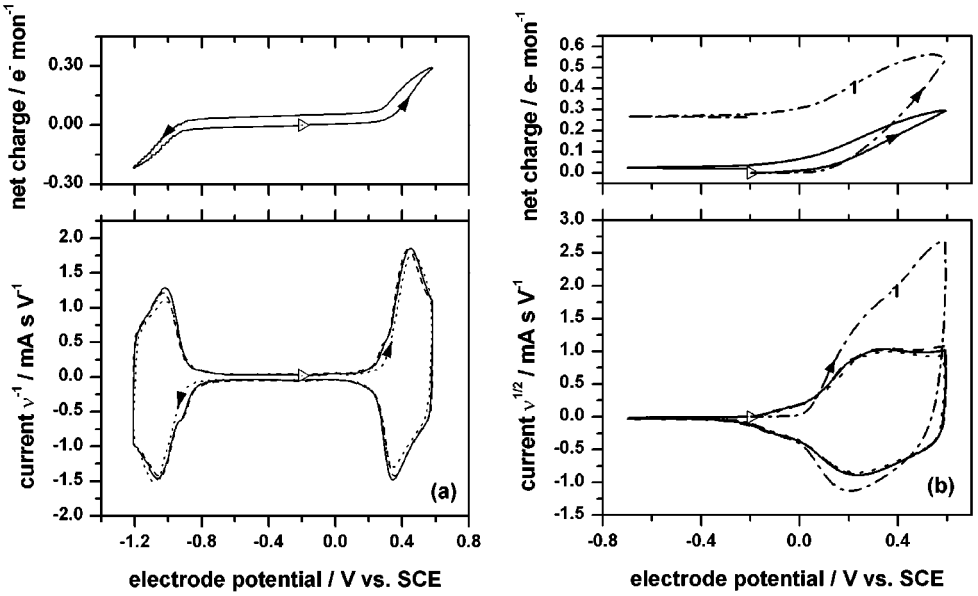

Figure 1. Single-electrode voltammetry data for ~1.5-μm films of (a) P_C and (b) P_A on glassy carbon electrodes in 0.075 M Me_4NBF_4. In both cases, the lower panel shows the cyclic voltammogram with the current linearly normalized by the scan rate υ. The solid, dashed, and dotted lines are for 20, 10, and 40 mV s^{-1}, respectively, collected in that order. For P_A, two scans were collected at the initial scan rate of 20 mV s^{-1} due to the observation of an initial break-in cycle (curve 1). The upper panel in both cases shows the charge calculated from direct integration of the voltammetric data collected at 20 mV s^{-1}. The charge calculated in this manner contains both Faradaic and non-Faradaic components and is expressed as electrons per mole of monomer unit. The open triangles denote the initial potential and direction of the scan, and the solid arrows clarify the path direction where necessary.

Electrochemical Methods. In all voltammetry experiments, anodic currents are reported as positive and cathodic currents as negative. All single working electrode voltammetry experiments were performed on ~1.5-μm thin films deposited on glassy carbon electrodes (Bioanalytic Systems, Inc., 3-mm diameter) in a single-compartment three-electrode geometry unless otherwise noted. Thin films were prepared by the deposition of 1 μL of a 5 mg mL^{-1} solution of methanol for P_A and DMSO for P_C. Voltammograms were collected using either a Solartron 1287 or 1286 potentiostat.

Dual working electrode voltammetry experiments were performed on 10−50-μm films sandwiched between a planar gold electrode and a gold micromesh (1500 lines in^{-1}, Buckbee Mears). The planar gold electrodes were fabricated by sequential deposition of a 5-nm Ti adhesion layer and a 50-nm Au layer on glass slides by thermal evaporation using a Key High Vacuum high-vacuum deposition chamber. A 0.12-cm^2 circular area was defined by adhering a 1.5-mm-thick glass cover slip, in which a 4-mm diameter circular hole had been drilled, using Tefzel (DuPont) as a hot-melt adhesize. The top of the cover slip was also coated with Tefzel to alter its wetting characteristics. P_A or P_C was solution cast by the dropwise addition of ~15 mg mL^{-1} saturated solutions in DMSO onto the exposed region of the gold electrode substrate. The final drop was used to imbed a circularly shaped (0.12 cm^2) gold micromesh. Extending from the circular region of the gold mesh was a small tail that extended onto the top of the glass cover slip mask and that was used for making electrical contact. The electrode was clamped to the O-ring joint of a previously described[28] two-compartment cell using a Kalrez O-ring. Electrical contact to the planar gold electrode was made by silver printing a wire to the gold substrate on a region not in contact with the interior of the electrochemical cell. Electrical contact to the gold mesh was realized by pressure contact of a platinum spring to its tail. Dual working electrode voltammetry experiments were performed using a either a Solartron 1287 or 1286 potentiostat to control the electrode potential (E) of the gold micromesh electrode (WE1) versus a reference electrode and measure the current, I_{aux}, through the auxiliary electrode. A Keithley 2400 Source-Measure unit was used to fix the E of the planar gold electrode (WE2) versus WE1 and measure the current, I_{WE2}, passing between WE2 and both WE1 and the auxiliary electrode.

A nonaqueous Ag(s) | Ag^+ reference electrode was used for all of the above experiments. It was constructed from a 3-mm-diameter glass tube to which a Vycor frit (Bioanalytical Systems, Inc.) was attached using polyethyelene heat shrink tubing. For voltammetry in Me_4NBF_4, a filling solution of 0.075 M Me_4NBF_4/0.005 M $AgNO_3/CH_3CN$ was used, and for voltammetry in Bu_4NBF_4, a filling solutions of 0.1M Bu_4NBF_4/0.005 M $AgNO_3/CH_3CN$ was used. The reference electrode potentials were measured versus a commercial saturated calomel electrode (SCE). For experiments conducted at electrolyte concentrations different from that of the reference electrodes employed, contributions from junction potentials were ruled out through voltammetry on ferrocene solutions.

Electrochemical quartz crystal microbalance (EQCM) studies were conducted on gold-coated AT-cut 10-MHz quartz crystals (International Crystal Manufacturing Co., Inc.). The metallized portion on one side of the quartz crystal was coated with a polymer film by solution deposition from DMSO. The coated quartz crystal was then sealed to the O-ring joint of an electrochemical cell. A silver wire pseudoreference and platinum wire coil auxiliary electrode were used for the EQCM studies. The frequency of the QC was measured using an oscillator circuit (International Crystal Manufacturing Co., Inc.) interfaced to a Tektronix TM5003 frequency counter with the polymer-coated electrode at ground. Simultaneous voltammetry was performed using a Solartron 1287 with the working electrode lead ungrounded at the instrument.

Results

A. Voltammetry of P_C in Small Ion Electrolytes. The lower panel of Figure 1a shows the single working electrode cyclic voltammogram of P_C collected in 0.075 M Me_4NBF_4/CH_3CN at three scan rates: 10, 20, and 40 mV s^{-1}. The voltammograms are linearly normalized by the scan rate, and the superposition of the normalized curves is consistent with the quasi-equilibrium electrochemistry of a surface-confined species. The E window is limited by the onset of deleterious redox chemistry (vide

(28) Zhou, X.; Langsdorf, B. L.; Jones, F. E.; Lonergan, M. C. *Inorg. Chim. Acta* **1999**, *294*, 207.

Table 1. Summary of Voltammetry Data for P_A and P_C in 0.075 M Me_4NBF_4[a]

	E_{pa} (P^+/P)	E_{pc}(P^+/P)	$E^{\circ\prime}$(P^+/P)	E_{pc}(P/ P^-)	E_{pa}(P/P^-)	$E^{\circ\prime}$(P/P^-)
P_C	0.45	0.35	0.40	−1.06	−1.02	−1.04
P_A	0.35	0.24	0.30			

[a] All potentials are in units of V vs SCE.

infra). The wave present at positive E corresponds to the oxidative or p-doping ($P \rightarrow P^+$) of the polymer, and the wave at negative E corresponds to the reductive or n-doping ($P \rightarrow P^-$) of the polymer.

As is typical for conjugated polymers, the voltammogram of P_C deviates from that expected for a simple surface-confined one-electron redox couple. First, the voltammetric waves are not symmetric. Although the anodic and cathodic peak potentials (E_{pa} and E_{pc}, respectively) are nearly identical for the n-doping (P/P^-) wave, they differ by 100 mV for the p-doping (P^+/P) wave (see Table 1). Second, the voltammogram tails to a constant-current plateau following the charging wave (for p-doping, this is more evident from the wider E range scan of Figure 4a) rather than returning to baseline levels. Finally, the peak width at half-maximum ($\Delta E_{p,1/2}$) is broader than expected for a simple one-electron redox couple; estimating from the first half of the charging waves (anodic for p-type and cathodic for n-type) yields $\Delta E_{p,1/2} \approx 200$ mV for both n-type and p-type doping.

The upper panel of Figure 1a shows the amount of charge, expressed as electrons per monomer unit (Chart 1 defines a monomer unit), derived from the simple integration of the voltammetric data. This integration includes both Faradaic and non-Faradaic charge, and consequently, it cannot be rigorously related to the doping stoichiometry. Rather, it represents an upper limit. The maximum doping level over the E range shown is therefore estimated to be ~0.3 e^-/monomer ≈ 12 double bonds/e^- [(C═C)/e^-] for the p-doping wave and ~0.25 e^-/monomer ≈ 16 (C═C)/e^- for the n-doping wave. The magnitude of the voltammograms, and hence these stoichiometry estimates, varied up to 20% between samples presumably due to the difficulty of accurately delivering the 1-μL deposition aliquots. It is noted that for both n- and p-type doping the net charge associated with the charging branches is ~15% greater than that observed upon discharge, as evidenced by the hysteresis in the top panel of Figure 1. All of the charge is accounted for, however, on a complete cycle through the n- and p-doping waves because of the similarity in the magnitude of the charging hysteresis observed for these two processes.

The cycling stability of P_C was extremely sensitive to the presence of dissolved oxygen, other impurities, and E range primarily due to deleterious overoxidation (vide infra). Under optimal conditions, a 1−2-μm film of P_C could be cycled through both the n-doping and p-doping waves with approximately a 1−2% loss in electroactivity per cycle over scan rates of 5−40 mV s^{-1}.

The presence of both fixed and mobile ions in the polymer film raises the possibility for a junction potential (Donnan potential) at the polymer | electrolyte interface. Figure 2a shows a series of voltammograms for the p-doping of P_C in varying concentrations of Bu_4NBF_4 in CH_3CN. The use of Bu_4NBF_4 in place of Me_4NBF_4 permitted preparation of higher concentration electrolyte solutions. The traces are normalized to account for

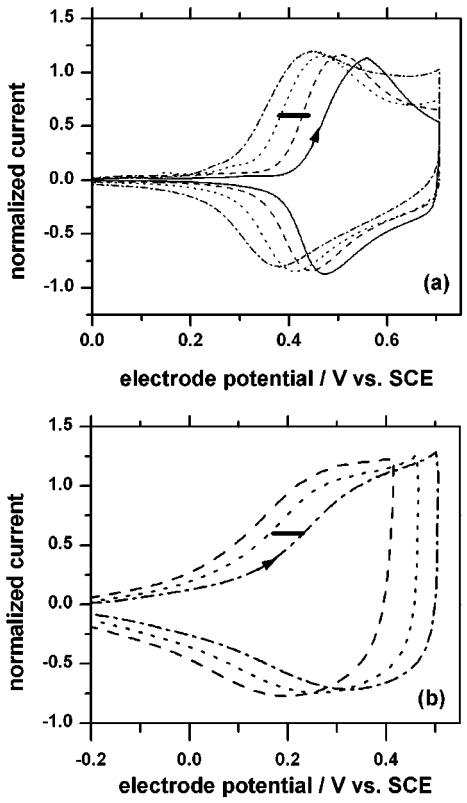

Figure 2. Electrolyte concentration dependence of the p-doping waves for (a) P_C and (b) P_A. The voltammograms were collected using ~1.5-μm films on glassy carbon electrodes (3-mm diameter) as a function of the concentration of Bu_4NBF_4 in CH_3CN used for the electrolyte: solid line, 0.001 M (P_C only); dashed line, 0.01 M; dotted line, 0.1 M; dash−dot line, 1 M. The scan rate for P_C was 2 mV s^{-1} and for P_A it was 10 mV s^{-1}. The length of the solid bar shown in each graph is 59 mV. Each set of concentration dependencies was collected using the same film, and the current is normalized to account for an ~15% decrease in intensity observed upon switching between electrolyte solutions. The scans were initiated at −0.3 V vs SCE, and the solid arrow indicates the path of the voltammograms.

a 15% loss in electroactivity that was observed upon switching electrolyte solutions. This loss of electroactivity did not result in a change in the shape of the voltammograms, and in terms of peak potentials, the results were independent of the concentration order in which they were collected. The voltammetric waves were observed to shift negative with increasing salt concentration. The magnitude of the shift is ~50 mV per order of magnitude change in electrolyte concentration. Similar results were observed for the n-doping wave.

Both the n- and p-doping waves for P_C are accompanied by an increase in the conductivity of the electrolyte-wetted film as demonstrated by dual-electrode voltammetry[29−31] on a polymer film sandwiched between a planar gold substrate (WE2) and a fine gold mesh (WE1). The E of WE2 and WE1 were swept versus the reference electrode while WE2 was held at 0.025 V relative to WE1. In Figure 3a, the lower panel shows the total current to the auxiliary electrode, I_{aux}, and corresponds to the typical single-electrode voltammogram. Despite the relatively slow scan rate (2 mV s^{-1}), the wave remains somewhat distorted

(29) Ofer, D.; Crooks, R. M.; Wrighton, M. S. *J. Am. Chem. Soc.* **1990**, *112*, 7869.
(30) Ofer, D.; Park, L. Y.; Schrock, R. R.; Wrighton, M. S. *Chem. Mater.* **1991**, *3*, 573−575.
(31) Dalton, E. F.; Surridge, N. A.; Jernigan, J. C.; Wilbourn, K. O.; Facci, J. S.; Murray, R. W. *Chem. Phys.* **1990**, *141*, 143−157.

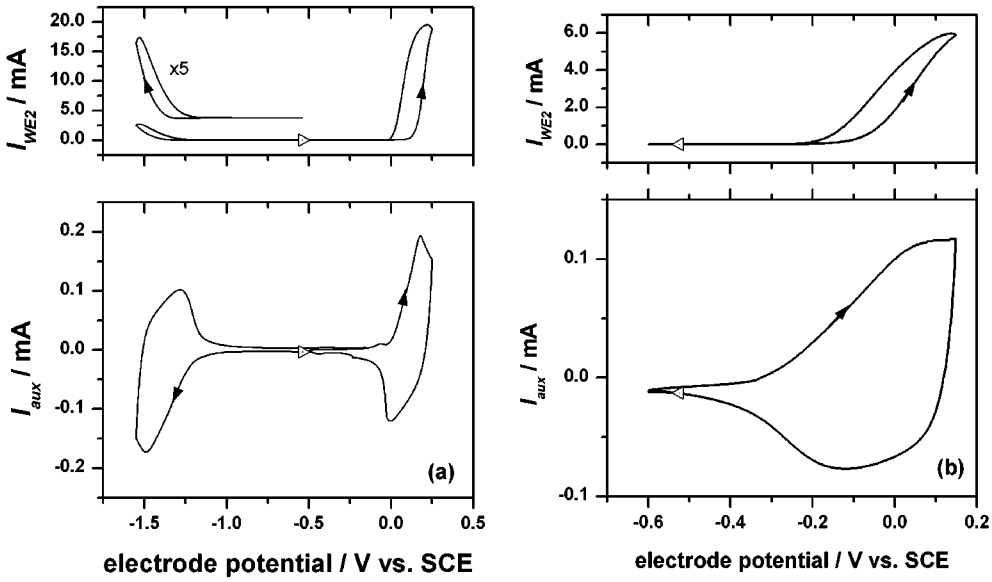

Figure 3. Dual-electrode voltammetry of ~50-μm films of (a) P_C and (b) P_A. In each case, the polymer film is sandwiched between a planar gold electrode (WE2) and a gold mesh electrode (WE1) in contact with 0.075 M Me_4NBF_4. The lower panel in each part shows the total current to the auxiliary electrode, which is dominated by the faradaic current from WE1 and WE2 to the auxiliary electrode and corresponds to net redox chemistry on the polymer film. The upper panel shows the current through WE2, I_{WE2}, which, for $I_{WE2} \gg I_{aux}$, is a measure of the electrical conductivity of the sample. The scan rate is 5 mV s^{-1}, and the electrode area is 0.1 cm^2. The open triangles denote the initial potential and direction of the scans, and the solid arrows clarify the path direction where necessary.

due to kinetic complications arising from the relatively thick film (~50 μm) used for this experiment. The upper panel of Figure 3a shows the sum of the current, I_{WE2}, passing between WE2 and WE1, and WE2 and the auxiliary electrode. As the film becomes conductive, the current due to electron transport through the polymer film between WE2 and WE1 dominates I_{WE2}, and it becomes a measure of the conductivity of the polymer film.[32] As shown in Figure 3a, P_C can be both n-type and p-type doped to a conductive state, with the n-type polymer 1 order of magnitude less conductive. The actual conductivity can only be crudely estimated due to the two-electrode configuration and somewhat ill defined geometry of the gold mesh. A crude estimate translates the 20-mA current observed in the p-doping wave to a conductivity of $3 \times 10^{-2}\ \Omega^{-1}\ cm^{-1}$, which is a lower limit due to the possibility of uncorrected contact resistances.

Sweeping P_C to more positive values of E than shown in Figure 1a results in a large chemically irreversible overoxidation with subsequent loss of electroactivity. Figure 4a shows voltammograms of P_C collected from -0.3 to $+1.6$ V versus SCE at 2, 10, and 40 mV s^{-1}. Although the overoxidation peak remains well separated from the reversible p-doping wave under the conditions investigated, it does shift closer to the reversible p-doping wave with decreasing scan rate. Simple integration of the voltammetric data, again uncorrected for the contribution from non-Faradaic processes, results in an estimated 3 e^-/monomer for the overoxidation peak.

B. Voltammetry of P_A in Small Ion Electrolytes. The anionically derivatized polymer, P_A, only shows a chemically reversible p-doping wave. Furthermore, P_A also exhibited a break-in period. Figure 1b shows single-working electrode voltammograms of P_A collected from -0.7 to 0.7 V versus SCE in 0.075 M Me_4NBF_4/CH_3CN at 10, 20 (2 cycles), and 40 mV

(32) It is not know at this time whether the conductivity is dominated by electronic (migration) or redox-type (diffusion) conduction.

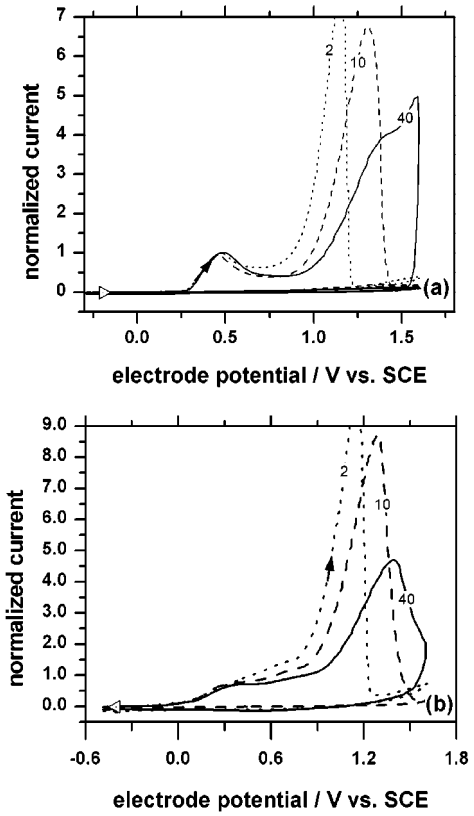

Figure 4. Single working electrode cyclic voltamograms for the oxidation of ~1.5-μm film of (a) P_C and (b) P_A on a glassy carbon (3-mm diameter) electrode in Me_4NBF_4 as a function of scan rate (as indicated by the curve labels): solid line, 40 mV s^{-1}; dashed, 10 mV s^{-1}; dotted line, 2 mV s^{-1}. For each scan rate, two cycles are shown with the second cycle difficult to discern as it is at baseline levels. The loss of electroactivity on sweeping to extreme positive potentials required that each pair of voltammograms be collected using a different polymer film. The voltammograms are normalized to the chemically reversible p-doping wave. The open triangles denote the initial potential and direction of the scans, and the solid arrows clarify the path direction where necessary.

s^{-1}. The curves are linearly normalized by scan rate. The first two cycles are at 20 mV s^{-1}. The anodic branch of the first cycle is larger than that observed for subsequent scans, with the cathodic branch being more similar. The superposition of the normalized voltammograms after the initial break-in sweep is consistent with the quasi-equilibrium electrochemistry of a surface-confined redox species. The voltammetry of P_A is somewhat broader than that of P_C. Although more poorly defined, the peak separation is on the order of 100 mV, similar to that observed for the p-doping wave of P_C. If the polymer was allowed to rest in its undoped state a break-in sweep was again observed.

The doping stoichiometry for the p-doping wave of P_A appears similar to that observed for P_C. The upper panel of Figure 1b shows the charge, expressed as e^-/monomer unit, calculated from simple integration of the voltammetric data. The break-in sweep exhibits a relatively large difference between the anodic and cathodic branches. Of the 0.6 e^-/monomer extracted on the anodic wave, only 0.3 e^-/monomer $\approx$ 12 (C═C)/e^- is returned on the cathodic branch. Subsequent sweeps show much less asymmetry with 90% of the 0.3 e^-/monomer extracted on the anodic charging branch being recovered on the cathodic discharging branch.

Under optimal conditions, the cycling stability of P_A is similar to that observed for P_C and a 1−2% loss in electroactivity was observed. The cycling stability, however, was more dependent on scan rate than with P_C. The loss in electroactivity per cycle increased as the scan rate decreased.

As with P_C, the voltammetry of P_A depends on electrolyte concentration, but the shift is observed to be in the opposite direction. Figure 2b shows cyclic voltammograms of P_A collected at 10 mV s^{-1} in 1, 0.1, and 0.01 M Bu_4NBF_4/CH_3CN. Again these curves were normalized to account for differences in scan rate and a slight loss of electroactivity upon switching electrolytes. Studies at electrolyte concentrations less than 0.01 M were not possible because of the contributions from overoxidation (vide infra) at the low scan rates required for low-conductivity dilute electrolytes. As the electrolyte concentration is reduced, the voltammograms shift in the positive direction. The shift is ~50 mV for each order of magnitude change in electrolyte concentration, similar to that observed for P_C.

Although a chemically reversible n-doping wave was not observed, a transient feature was observed in the voltammograms of P_A upon driving to *E* values negative of −1.0 V versus SCE in Me_4NBF_4/CH_3CN. Figure 5 shows the voltammogram of P_A first swept between −1.5 and +0.6 V versus SCE for three cycles (top panel) and then through the range −0.3 to +0.6 V versus SCE (bottom panel). The sweep is initiated through the p-doping wave, resulting in a voltammogram similar to that in Figure 1b. Upon sweeping *E* negative of −1.0 V versus SCE, a feature is evident, and the subsequent p-doping wave narrows and shifts toward positive potentials (Figure 5, top panel). The narrower p-doping wave persists as long as it is preceded by passage through potentials negative of −1.0 V versus SCE. Continued cycling over this wide *E* range results in a continual positive shift of the narrowed p-doping wave and a decrease in the magnitude of the feature observed at negative *E*. The original behavior of the polymer can be recovered and the polymer "reset" by cycling through only the p-doping wave as shown in the lower panel of Figure 5. Similar behavior is also observed for P_A in Bu_4NBF_4, but more negative values of *E* are required to either see a feature or induce a change in the p-doping wave.

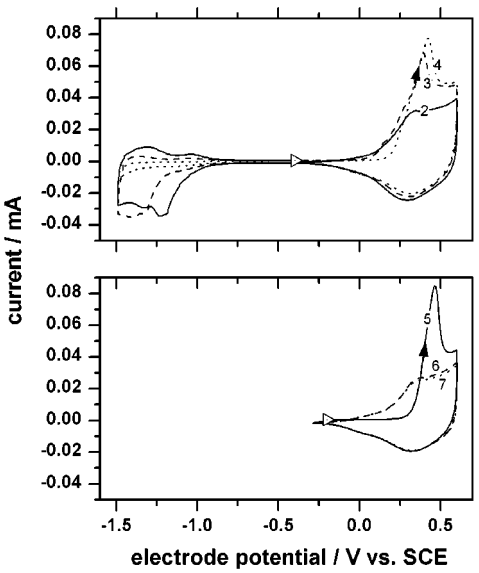

Figure 5. Cyclic voltammograms of P_A (0.092 mg) on a glassy carbon electrode (3-mm diameter) in 0.075 M Me_4NBF_4/CH_3CN. The polymer was first cycled once between −0.3 and +0.6 V vs SCE as a break-in cycle (not shown). The upper panel shows the next three scans over the potential range −1.5 to +0.6 V vs SCE, and the lower panel the subsequent three scans over the narrower potential range of −0.3 to +0.6 V vs SCE. The small numbers labeling the curves indicate the scan number, with again the first scan omitted. The open triangles denote the initial potential and direction of the scans, and the solid arrows clarify the path direction where necessary.

The feature observed at negative *E* did not result in the film becoming electrically conductive. Only the chemically reversible p-doping wave imparted conductivity to the film. Figure 3b shows the dual-electrode voltammetry for a film of P_A sandwiched between planar gold and gold mesh electrodes. Given a similar geometry and film thickness, the currents observed indicate that the two-electrode measured conductivities observed for P_A were similar to those measured for P_C.

As with P_C, driving P_A to extreme positive *E* results in a large overoxidation peak and a complete loss of electroactivity. Figure 4b shows cyclic voltammograms of P_C collected from −0.3 to +1.6 V versus SCE at 2, 10, and 40 mV s^{-1}. Relative to P_C, the overoxidation peak for P_A appears to have more of a leading edge that tails into the reversible p-doping wave making it less well defined. The onset of this leading edge and the peak current shift negative as the scan rate decreases.

C. Electrochemical Quartz Chemical Microbalance Studies. Figure 6 shows the results of EQCM studies[33,34] for the n-doping of P_C and the p-doping of P_A in 0.1M Bu_4NBF_4/CH_3CN. These particular waves are the focus because they can potentially lead to the internally compensated state. The voltammograms shown in the upper panels are somewhat distorted relative to those shown in Figure 1 because of the relatively thick films necessary for adequate signal/noise in the QCM measurement. The lower panels of Figure 6 compare the frequency change, Δf, of the QC to the charge calculated from integrating the voltammograms. The Δf traces qualitatively trace

(33) Kanazawa, K. K.; Melroy, O. R. *IBM J. Res. Dev.* **1993**, *37*, 157−171.
(34) Ward, M. D. In *Principles and Applications of the Electrochemical Quartz Crystal Microbalance.*; Rubinstein, I., Ed.; Dekker: New York, 1995.

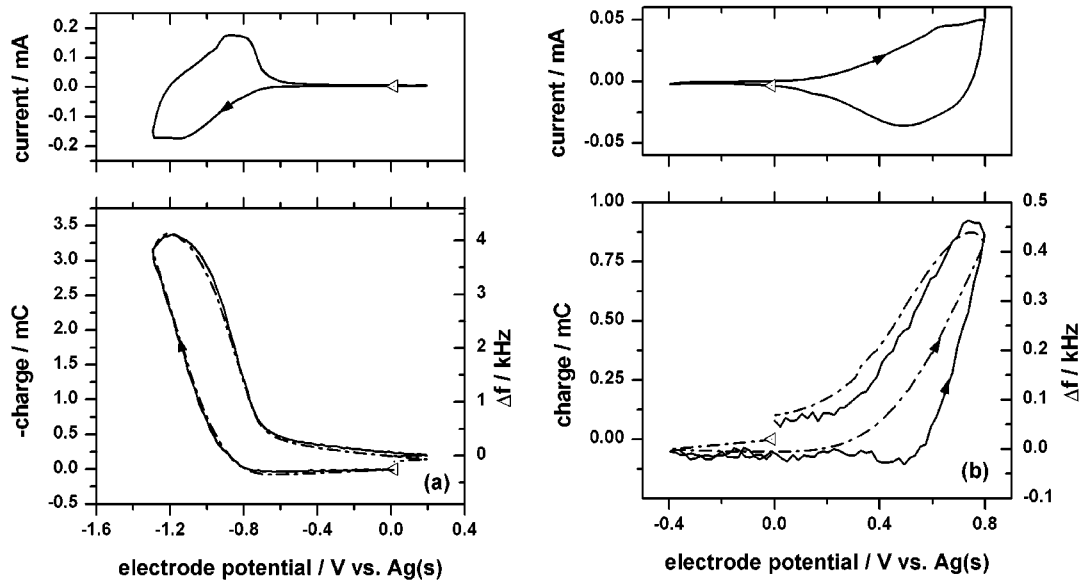

Figure 6. EQCM results for (a) P_C and (b) P_A collected in 0.1 M Bu_4NBF_4/CH_3CN at 20 mV s^{-1}. The top panel in each part shows the voltammogram. The bottom panel shows the simultaneously collected frequency change (solid line, left ordinate) of the gold-coated, polymer-modified quartz crystal and the integrated charge from the voltammogram (dash−dot line, right ordinate). The open triangles denote the initial potential and direction of the scans, and the solid arrows clarify the path direction where necessary.

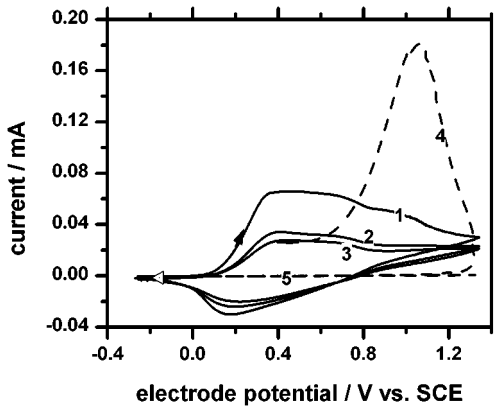

Figure 7. Cyclic voltammogram of a 1.5-μm film of P_A on glassy carbon collected first in Bu_4NPSS (solid line, scans 1−3) and then in Bu_4NBF_4 (dashed line, scans 4 and 5). The small numbers indicate the scan number, and the fifth scan is essentially at baseline levels. The open triangles denote the initial potential and direction of the scans, and the solid arrows clarify the path direction where necessary.

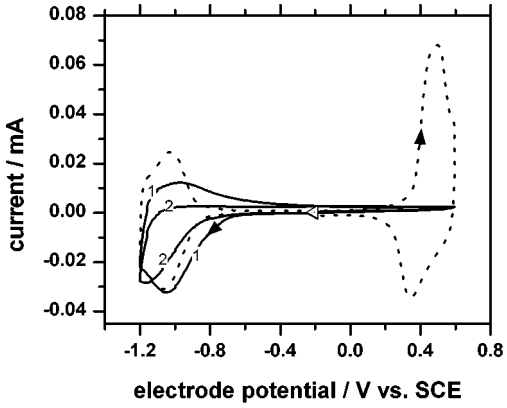

Figure 8. Cyclic voltammograms of a 1.5-μm film of P_C on a glassy carbon electrode (3-mm diameter) first collected in Bu_4NPSS (2 cycles, solid lines) and then in Bu_4NBF_4 (1 cycle, dotted line). The numbers indicate the scan number for the sweeps in Bu_4NPSS, and the open triangle indicates the initial potential and scan direction. The solid arrows clarify the path direction where necessary.

the integrated charge, and the increase in frequency observed upon doping is consistent with a decrease in the mass of the polymer film and the formation of the internally compensated state. The QCM data are only considered qualitatively. Reliable quantification of these data, for instance to extract the doping stoichiometry, requires a more detailed impedance analysis[35−39] that we have not performed.

D. Electrochemistry of P_A in Bu_4NPSS. Figure 7 shows the voltammogram of a P_A film first swept in Bu_4NPSS (3 cycles) and then in Bu_4NBF_4 (2 cycles) under otherwise identical conditions. The large overoxidation peak characteristic of the electrochemistry of P_A in small-molecule electrolytes is not observed. The first cycle in Bu_4NPSS exhibits the break-in sweep discussed above, and the second two sweeps demonstrate that the polymer can be swept to large positive E without a complete loss of electroactivity. When the same film is transferred to Bu_4NBF_4 and swept over the same E window, a large overoxidation peak is observed accompanied by a complete loss of electroactivity, as observed above. Integration of the voltammetry data in Bu_4NPSS, again assuming only Faradaic current, results in an estimated depth of charge of 1.1 e^-/monomer on the first break-in sweep and 0.6 e^-/monomer on the second sweep. It is noted that the voltammetry in Figure 7 exhibits kinetic complications in that anodic currents persist even after the scan direction is switched from positive to negative at $E =$ 1.3 V versus SCE.

E. Electrochemistry of P_C in Bu_4NPSS. Figure 8 shows the voltammogram of a P_C film first swept in Bu_4NPSS (2 cycles) and then in Bu_4NBF_4 (1 cycle). In Bu_4NPSS, the p-doping wave is completely absent, and the n-doping wave is highly distorted

(35) Muramatsu, H.; Tamiya, E.; Karube, I. *Anal. Chem.* **1988**, *60*, 2142−2146.
(36) Martin, S. J.; Granstaff, V. E.; Frye, G. C. *Anal. Chem.* **1991**, *63*, 2272−2281.
(37) Fruboses, C.; Doblhofer, K. *Synth. Met.* **1993**, *55*, 1329−1334.
(38) Reed, C. E.; Kanazawa, K. K.; Kaufman, J. H. *J. Appl. Phys.* **1993**, *68*, 1993−2001.
(39) Noel, M. A. M.; Topart, P. A. *Anal. Chem.* **1994**, *66*, 484−491.

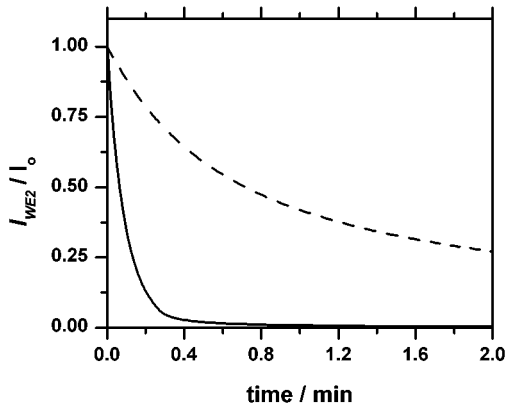

Figure 9. I_{WE2} following a potential step from −1.2 to −0.7 V vs SCE for a film of P_C sandwiched between a planar gold electrode (WE2) and a gold mesh electrode (WE1) in contact with either Bu_4NBF_4 (solid line) or Bu_4-NPSS (dashed line). Prior to this potential step at $t = 0$ min, the potential was held at −1.2 V vs SCE for 6 min. During the time period shown, E_{WE1} was held at −0.7 V vs SCE and E_{WE2} was held at 0.025 V vs E_{WE1}.

and appears irreversible. Furthermore, the magnitude of the n-doping wave decreases upon subsequent cycling. This large change in sequential cycles and apparent irreversibility of the n-doping process in Bu_4NPSS is not primarily due to chemical degradation. This is evidenced by the subsequent voltammogram of the same film in Bu_4NBF_4 that is similar to those shown in Figure 1a. Furthermore, if chemical degradation were primarily responsible for the irreversibility of the doping waves, the formation of an electrically conductive film may not be expected. Nonetheless, as in the small ion electrolytes, the n-doping wave in Bu_4NPSS results in an increase in conductivity.

The above results suggest that the asymmetry of the n-doping wave is due to a kinetically slow reoxidation to the neutral undoped form. Indeed, upon sweeping through the n-doping wave and back to $E = -0.8$ V versus SCE in Bu_4NPSS/CH_3CN, the E of P_C will quickly drift negative upon removal of potentiostatic control. To further explore the kinetics of the reoxidation process, a dual electrodepotential step experiment was performed. The E of WE1 was first stepped to −1.5 V versus SCE for 6 min to n-dope the polymer. The E of WE1 was then stepped to −0.8 V versus SCE while maintaining a 0.025-V potential difference between WE1 and WE2. The I_{WE2} while the P_C was being held at −0.8 V versus SCE is shown in Figure 9 as a function of time. In Bu_4NBF_4 / CH_3CN, I_{WE2} rapidly decays to background levels as the material is undoped. In Bu_4NPSS/CH_3CN, however, the conductivity drops more slowly (I_{WE2} remains nonzero), and the film remains electrically conductive even after 10 min of driving to −0.8 V versus SCE.

F. Voltammetry of P_C | P_A Bilayer Structures. Due to the interest of using polyelectrolyte-mediated electrochemistry in the preparation of interfaces between dissimilarly doped conjugated polymers, the voltammetry of a bilayer structure of P_C and P_A was investigated. A film of P_C was solution cast from DMSO onto a planer gold electrode (WE2) followed by solution casting of P_A from methanol (P_C is insoluble in methanol). A fine gold mesh (WE1) was imbedded in the P_A layer to enable dual-electrode voltammetry. The lower panel of Figure 10 shows I_{aux} for this bilayer structure as the E of WE2 and WE1 are swept while maintaining WE2 at 0.025 V versus WE1. The upper panel shows I_{WE2}, which as described above contains a contribution from the electrical conduction between WE1 and

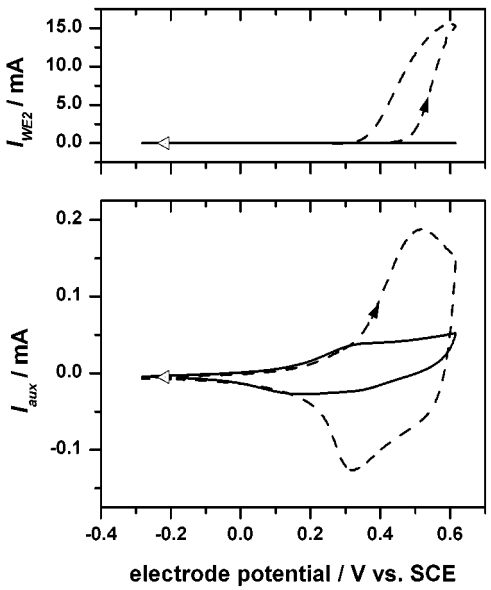

Figure 10. Dual-electrode voltammetry data on a planar gold electrode (WE2) | P_C | P_A | gold mesh (WE1) polymer bilayer structure in 0.1 M Bu_4NPSS/CH_3CN (solid line) and 0.1 M Bu_4N BF_4/CH_3CN (dashed line). The lower panel shows the current from WE2 and WE1 to the auxiliary electrode, I_{aux}, and the upper panel shows the current through WE2, I_{WE2}, which for $I_{WE2} > I_{aux}$ is a measure of the conductivity of the bilayer film. The scan rate was 5 mV s^{-1}.

WE2. The bilayer was first swept in Bu_4NPSS/CH_3CN and then in Bu_4NBF_4/CH_3CN. In Bu_4NPSS/CH_3CN, the bilayer film remains insulating and a voltammogram corresponding to the p-doping of P_A is observed. This argues that P_A is being selectively oxidized with the formation of a p-doped layer of P_A on top of an undoped layer of P_C. The subsequent scan in Bu_4NBF_4/CH_3CN over the same E range shows a larger voltametric wave corresponding to the oxidation of both P_C and P_A as well as an increase in the conductivity of the bilayer structure.

Discussion

A. Electrochemical Doping. The electrochemical doping of P_C is typical of polyacetylene and other poly(RCOT)s, which can be both n- and p-type doped.[40] P_A, however, is unusual in that it can be only p-doped. The absence of an n-doping wave for P_A is somewhat surprising given its structural similarity to P_C and other poly(RCOT)s. The λ_{max} in the visible absorption spectra of P_A and P_C are similar,[8] and based on these data, P_A would be expected to show an n-doping wave at potentials similar to P_C. The absence of an n-doping wave in P_A is not understood.

The depth of charging [12−16 (C═C)/e^-] accompanying the reversible doping of P_C and P_A is similar to that reported for other poly(RCOT)s.[40] For both P_A and P_C, the integrated charging branch is 10−15% larger than the discharging branch. Over an entire n-doping and p-doping cycle of P_C, however, the anodic and cathodic charge balance to within 1% of the maximum charge extracted during the doping process. This argues that the observed hysteresis is due to charge trapping. Some residual charge from each doping process is not released until passage through the opposite doping process. Similar

(40) Jozefiak, T. H.; Ginsburg, E. J.; Gorman, C. B.; Grubbs, R. H.; Lewis, N. S. *J. Am. Chem. Soc.* **1993**, *115*, 4705−4713.

effects have been observed for instance in polythiophenes where charge-trapping effects are argued to manifest themselves in so-called prepeaks preceding the doping waves.[41,42] The implication of charge-trapping effects over an irreversible chemical degradation is also supported by the fact that the 10−15% charging hysteresis on a single doping wave does not result in a similar level of decrease on subsequent sweeps. The loss in electroactivity on subsequent sweeps is only 1−2%.

As is typical with conjugated polymers, the doping waves of P_A and P_C deviate from the predictions of an ideal one-electron surface-bound redox couple.[43,44] The $\Delta E_{p,1/2} \approx 200$ mV for P_C and even larger $\Delta E_{p,1/2}$ for P_A are much larger than expected for such an ideal surface couple and also larger than reported for other poly(RCOT)s, which exhibit $\Delta E_{p,1/2} = 50 \pm 5$ mV for charging waves and $\Delta E_{p,1/2} = 80 \pm 5$ for discharging waves.[40] The value of $\Delta E_{p,1/2}$ for P_C is still narrow for conjugated polymers and that for P_A is more typical. The broad doping waves exhibited by conjugated polymers are typically argued to be due to a distribution of states. Such a distribution has also been suggested as an explanation for the tailing of the voltammograms to a capacitive-like charging region at large values of $|E|$.[45] The explanation of this effect has been controversial, however, with true capacitive charging being a common competing explanation.[46,47]

The scan rate-independent separation between E_{pa} and E_{pc} is negligible for the n-type doping of P_C and on the order of 100 mV for the p-type doping of P_A or P_C. The nonzero separations between E_{pa} and E_{pc} observed for the p-doping wave are inconsistent with the predictions of an ideal surface-bound redox couple. The scan rate independence argues that the separation is not due to slow heterogeneous electron-transfer kinetics, which is an explanation for separation between E_{pa} and E_{pc} observed with conjugated polymers under certain conditions.[48] As with other poly(RCOT)s, the separation is small relative to that observed for many conjugated polymers where nonzero peak separations have been argued to be due to relaxation effects.[49−51] The essentially neglible peak separation observed for the n-doping of P_C is unusual for conjugated polymers and indicates minimal structural reorganization upon n-type doping.

As with other ionically functionalized conjugated polymers[15,16] and conjugated polymer/polyelectrolyte blends,[10−14] doping of both P_A and P_C proceed with the formation of the internally compensated state where possible. The EQCM data (Figure 6) support the loss of cations upon the p-doping of P_A and the loss of anions upon the n-doping of P_C. This is not surprising given that the swollen polymer is not likely to solvate ion pairs nearly as well as CH_3CN. Based on coulometry data, the level of reversible charging remains substantially below (<0.3 e^-/monomer) the maximum that could be compensated by the covalently bound ionic centers. Consequently, no change in the mechanism of charge compensation is observed in the EQCM data as has been observed for other ionically functionalized electroactive polymers.[52] Although a number of internally compensated p-type polymers have been reported,[17−23] there are relatively few examples of n-type internally compensated polymers.[53]

B. History Effects. A common aspect of the voltammetry of conjugated polymers is a dependence on their electrochemical history. In particular, P_A exhibits a rich array of history effects. Most notable is the presence of a break-in wave. Such break-in waves are commonly observed for a range of conjugated polymers and have been argued to be due to *slow* relaxation effects.[54−56] In addition to a break-in wave, P_A also exhibited a change in the p-doping wave upon sweeping through negative potentials. The resulting p-doping wave is sharper than either the relaxed (break-in) or steady-state waves of Figure 1b. Undoubtedly, the complete description of this history effect is complex.The dependence on electrolyte size of the E required to change the nature of the p-doping suggests that this effect may be due to the reorganization of ions, with the shift in the p-doping wave perhaps due to a redistribution of space charge within the polymer. The involvment of ions is supported by the observation of current that is not accompanied by an increase in the conductivity at negative E.

C. Dependence on Electrolyte Concentration. A dependence of the voltammograms on electrolyte concentration is expected for polyelectrolytes due to the selective partitioning of ions across the polymer | electrolyte interface.[43] Such effects have been explored in both ionically functionalized conjugated polymers and blends of conjugated polymers with non-redox-active polyelectrolytes.[57,58] For P_A, E_{pa} and E_{pc} shift negative as the electrolyte concentration decreases (Figure 2b). At dilute electrolyte concentration, the concentration gradient at the polymer | electrolyte interface will result in the transfer of ions from the polymer to the electrolyte. As only the cations in P_A can pass into the electrolyte, a Donnan potential develops with the polymer acquiring a net negative charge. The lower the electrolyte concentration, the greater the negative charge acquired and the easier it becomes to oxidize the polymer. Consequently, the E_{pa} and E_{pc} shift negative with decreasing electrolyte concentration. Exactly the reverse behavior is observed for the cationic polymer as would be expected for the selective partitioning of anions. In both cases, the shift is 50 mV per decade change in electrolyte molarity, which is slightly less than the 59 mV expected for an ideal solution, perhaps due to neglected activity corrections.[59]

D. Formal Potentials. The presence of a Donnan potential makes it difficult to determine the true formal potentials for

(41) Crooks, R. M.; Chyan, O. M. R.; Wrighton, M. S. *Chem. Mater.* **1989**, *1*, 2−4.
(42) Borjas, R.; Buttry, D. A. *Chem. Mater.* **1991**, *3*, 872−878.
(43) Doblhofer, K.; Rajeshwar, K. In *Electrochemistry of Conducting Polymers*; Skotheim, T. A., Elsenbaumer, R. L., Reynolds, J. R., Eds.; Marcel Dekker: New York, 1998; pp 531−588.
(44) Pickup, P. G. *Mod. Aspects Electrochem.* **1999**, *33*, 549−597.
(45) Heinze, J.; Storzbach, M.; Mortensen, J. *Ber. Bunsen-Ges. Phys. Chem.* **1987**, *91*, 960−967.
(46) Feldberg, S. W. *J. Am. Chem. Soc.* **1984**, *106*, 4671−4674.
(47) Cai, Z.; Martin, C. R. *J. Electroanal. Chem.* **1991**, *300*, 35−50.
(48) Vorotyntsev, M. A.; Daikhin, L. I.; Levi, M. D. *J. Electroanal. Chem.* **1992**, *332*, 213−235.
(49) Heinze, J.; Bilger, R.; Meerholz, K. *Ber. Bunsen-Ges. Phys. Chem.* **1988**, *92*, 1266−1271.
(50) Albery, W. J.; Chen, Z.; Horrocks, B. R.; Mount, A. R.; Wilson, P. J.; Bloor, D.; Monkman, A. T.; Elliot, C. M. *Discuss. Faraday Soc.* **1989**, *88*, 247−259.
(51) Meerholz, K.; Heinze, J. *Angew. Chem., Int. Ed. Engl.* **1990**, *29*, 692−695.
(52) Qiu, Y.-J.; Reynolds, J. R. *J. Electrochem. Soc.* **1990**, *137*, 900−904.
(53) Zhang, N.; Wu, R.; Li, Q.; Pakbaz, K.; Yoon, C. O.; Wudl, F. *Chem. Mater.* **1993**, *5*, 1598−1599.
(54) Odin, C.; Nechtschein, M. *Synth. Met.* **1991**, *44*, 177−88.
(55) Odin, C.; Nechtschein, M. *Phys. Rev. Lett.* **1991**, *67*, 1114−1117.
(56) Odin, C.; Nechtschein, M.; Hapiot, P. *Synth. Met.* **1992**, *47*, 329−350.
(57) Zhong, C.; Doblhofer, K.; Weinberg, G. *Discuss. Faraday Soc.* **1989**, *88*, 307−316.
(58) Zhong, C.; Storck, W.; Doblhofer, K. *Ber. Bunsen-Ges. Phys. Chem.* **1990**, *94*, 1149−1155.
(59) Braun, H.; Storck, W.; Doblhofer, K. *J. Electrochem. Soc.* **1983**, *130*, 807−811.

the doping of P_A and P_C because rigorously assigning formal potentials requires knowledge of the relevant ion activities. The assignment of formal reduction potentials is also complicated by the nonzero quasi-equilibrium separations between E_{pa} and E_{pc} and the broad peaks (in particular for P_A) which are not in agreement with the predictions for a surface-bound one-electron redox couple. Due to the complications noted above, only apparent formal potentials, defined as $E^{\circ\prime} = (E_{pa} + E_{pc})/2$ as measured in 0.075 M Me_4NBF_4/CH_3CN, are reported (see Table 1). The choice of this electrolyte in tabulating $E^{\circ\prime}$ is for comparison to other poly(RCOTs) where voltammetry is reported in Me_4NBF_4/CH_3CN.

The values $E^{\circ\prime}(P^+/P)$ in 0.075 M M Me_4NBF_4/CH_3CN for P_A and P_C are similar (see Table 1), and in fact, the 100-mV difference could be due simply to Donnan potential effects. The dependence of $E^{\circ\prime}$ on substituent depends both on steric interactions that alter the conjugation length of the polyacetylene backbone and on inductive or resonant electronic effects. Steric interactions that can result in a very strong dependence of $E^{\circ\prime}$ on substituent for many conjugated polymers are somewhat minimized in poly(RCOT)s due to the relatively low substituent density. Consequently, the $E^{\circ\prime}$ for poly(RCOT)s, including P_A and P_C, varies over a relatively narrow range ($\sim$300 mV). The electronic influence of the substituents on P_A and P_C are expected to be similar because of the presence of two methylene groups between the backbone and the sulfonate or alkylammonium moieties. In fact, the $E^{\circ\prime}(P^+/P) = 0.39$ V versus SCE for simple alkyl-substituted poly(*n*-butylCOT) is similar to that observed for P_A and P_C.[40]

The $E^{\circ\prime}(P/P^-)$ for P_C is the most positive of any of the poly(RCOT)s that have been reported, and the separation $E^{\circ\prime}(P^+/P) - E^{\circ\prime}(P/P^-) = 1.44$ V is the smallest reported for any poly(RCOT). These observations are consistent with the fact that P_C also exhibits among the lowest energy optical absorption maximum ($\lambda_{max} = 614$ nm) of any poly(RCOT) in solution.[60,61] These results indicate a very high degree of conjugation for P_C.

E. Cycling Stability and Overoxidation. The cycling stabilities of P_C and P_A are similar to that reported for other poly(RCOT)s with an $\sim$1% decrease in the intensity of the steady-state voltammetry per cycle under optimal conditions. The sensitivity of the cycling stability of P_A to scan rate over the range studied appears closely coupled to overoxidation of the polymer. As with polyacetylene[62] and a range of conjugated polymers,[63−65] poly(RCOT)s exhibit a deleterious overoxidation process. The loss of electroactivity that results from overoxidation has been argued to be due to nucleophilic subsitution reactions with trace water or other nucleophiles.[63] For P_A, the leading edge of the overoxidation peak competes thermodynamically with the chemically reversible p-doping wave, although it is kinetically slower as evidenced by the scan rate dependence of Figure 4b. At fast scan rates, the kinetics of the overoxidation result in a negligible degradation, whereas at slower scan rates, the overoxidation competes with the reversible p-doping resulting in poorer cycling stability and presumably poorer long-term stability. For P_C, the overoxidation did not compete effectively with the reversible p-doping over the range of scan rates studied, resulting in better cycling stability over a wider range of scan rates. The fact that the overoxidation peak continues to shift negative even at the slowest scan rates studied indicates, however, that it may still compete on a thermodynamic basis and is perhaps only separated because of kinetic effects. The overoxidation peak has generally been observed to be well separated from the reversible p-doping wave for other poly(RCOT)s.[40]

F. Self-Limiting Oxidation with Bu_4NPSS. Complete overoxidation of P_A requires injecting a density of charge greater than can be compensated by the density of covalently bound ionic functionalities. In contrast to charge compensation occurring by the loss of cations that is observed at low p-doping levels, the overoxidation of P_A is expected to occur with the eventual incorporation of anions to accommodate the 3 e^-/monomer charging level. In Bu_4NPSS/CH_3CN, the large PSS^- anion is not expected to permeate the polymer film, and the level of oxidation should be limited to the density of mobile cations in the polymer (1 e^-/monomer) thereby inhibiting overoxidation. Indeed, the voltammetry of P_A in Bu_4NPSS/CH_3CN does not show the large overoxidation peak that is observed in the small ion electrolyte Me_4NBF_4/CH_3CN (see Figure 7). This suggests that the p-doping of P_A in Bu_4NPSS is self-limiting. The coulometry data also support this conclusion. The upper limit on the anodic charge extracted on the initial, relaxed p-doping wave is estimated to be 1.1 e^-/monomer unit. It is emphasized that such self-limiting electrochemistry is only possible with the appropriate *combination* of both redox-active and inert electrolyte polyions.

The self-limiting electrochemistry of P_A suggests that it is possible to control the level of doping through polymer structure, namely, the density of ionic functionalities. The usual approach to precise control of the doping level is through control of E. The self-limiting electrochemistry possible with conjugated ionomers offers two significant advantages. First, the doping level can be limited regardless of the potential. This effectively expands the potential range over which conjugated polymers can be used. For instance, in the case of P_A, large positive potential excursions can be conducted without complete loss of electroactivity. Second, self-limiting electrochemistry provides a means of preparing the precisely internally compensated state where the charge injected into the polymer backbone is precisely balanced by the density of charge covalently bound to the polymer backbone in the form of ionic functionalities. In the context of device application, the precisely internally compensated state may be particularly interesting because of the absence of any highly mobile ions. The control of mobile ion density is especially important in controlling the electrostatic potential profile through the polymer or, equivalently, the distribution of space charge.

G. Selective Doping and the Fabrication of Interfaces between Dissimilarly Doped Conjugated Polymers. In early studies on the electrochemistry of conjugated polymers, it was recognized that the kinetics for doping depends heavily on the

(60) Gorman, C. B.; Ginsburg, E. J.; Grubbs, R. H. *J. Am. Chem. Soc.* **1993**, *115*, 1397−1409.
(61) Comparison to UV/visible data of ref 60 is somewhat complicated by the fact that different solvents were utilized, and in some cases, the polymer "solutions" contained solid material that reportedly did not filter through a 0.4-μm filter.
(62) Chien, J. C. W.; Schlenoff, J. B. *Nature* **1984**, *311*, 362−3.
(63) Beck, F.; Braun, P.; Oberst, M. *Ber. Bunsen-Ges. Phys. Chem.* **1987**, *91*, 967−974.
(64) Krische, B.; Zogorska, M. *Synth. Met.* **1989**, *28*, C257−63.
(65) Tsai, E. W.; Basak, S.; Ruiz, J. P.; Reynolds, J. R.; Rajeshwar, K. *J. Electrochem. Soc.* **1989**, *136*, 3683−3689.

size of the electrolyte employed ("ion sieving").[66,67] The electrolyte Bu_4NPSS represents an extreme in the spectrum of electrolyte size. Consequently, it can be used to completely suppress the oxidative electrochemistry of conjugated polymers, as observed with P_C (see Figure 8). The p-doping of P_C requires the incorporation of a charge-compensating anion that cannot be provided by PSS^- due to its low permeability. In contrast, the use of a polyanion does not suppress the oxidative electrochemistry of P_A (see Figure 7) because it has a built-in means of charge compensation. Consequently, through the appropriate choice of ionically functionalized conjugated polymer and inert polyelectrolyte, it is possible to perform *selective* redox chemistry on one of two materials that have similar values of $E^{\circ\prime}$.

The possibility for selective redox chemistry is a useful tool in preparing conjugated polymer "homojunctions" that may be interesting for device applications. It is particularly significant given the general insolubility of doped conjugated polymers. Such insolubility means that it is often more convenient to prepare structures via solution casting of undoped conjugated polymers that tend to exhibit much greater solubilities than their doped counterparts. With selective redox chemistry, it is possible to cast a series of undoped polymers with similar $E^{\circ\prime}$ values and then selectively oxidize or reduce specific regions to introduce interfaces between dissimilarly doped conjugated polymers. Indeed, the studies presented on the bilayer P_C | P_A structure show the preparation of the simplest such interface by selective oxidation, namely, the interface between a doped conjugated polymer and an undoped conjugated polymer (see Figure 10).

H. Inhibiting the Reoxidation of the n-Doped State. The use of a polyanion electrolyte can not only suppress oxidation to the p-doped state but also inhibit reoxidation of the n-doped state back to its neutral form. The voltammograms for the n-doping of P_C in Bu_4NPSS/CH_3CN are highly distorted with the anodic discharging branch being smaller than the cathodic charging branch (see Figure 8). As demonstrated by EQCM, the reduction of P_C occurs with the loss of anions, $CF_3SO_3^-$ in this case. In Bu_4NPSS, the only ions available for reoxidation to the undoped state are the $CF_3SO_3^-$ lost from the polymer film. The availability of these counterions is limited, however, by their diffusion into the bulk of the electrolyte solution. Consequently, complete reoxidation will not be suppressed, resulting in an asymmetric voltammogram with a decrease in intensity upon subsequent sweeps. The decrease in intensity is not due to degradation as evidenced by the recovery observed when placed in a Bu_4NBF_4/CH_3CN.

The voltammetry of P_C in Bu_4NPSS bears some analogy to electrochemical stripping experiments and could be termed "ion stripping". The slow reoxidation of P_C from its n-doped state corresponds to a preconcentration step whereby ions at low concentration in the electrolyte are concentrated into the modified electrode; the undoped polymer is already "preconcentrated". Upon reduction to the n-type form, the ions are stripped from the film and diluted into the electrolyte.

Inhibiting the reoxidation of the n-doped state is potentially useful in the introduction of both n- and p-doped regions in the same structure. The use of a macroanion electrolyte makes it in principle possible to drive a structure to oxidizing potentials to introduce a p-doped region without loss of a previously introduced n-type region, thereby providing a possible means to fabricate a pn junction. The slow kinetics for the undoping of n-type P_C in Bu_4NPSS/CH_3CN relative to Bu_4NBF_4/CH_3CN observed in dual electrode potential step experiments (Figure 9) supports this assertion. Presumably, the density of available anions limits the kinetics for the reoxidation of n-type P_C to its undoped form. In this case, the concentration of small anions in the electrolyte is determined by impurities and those anions lost from the polymer film upon initial n-doping.

Summary

The polymers P_C and P_A are excellent candidates for exploring doped conjugated polymer homojunctions because they provide for both internally compensated, conductive, n- and p-type forms. The voltammetry of P_C is qualitatively similar to the voltammetry of other poly(RCOT)s with the observation of both n- and p-doping waves that are relatively narrow and well-defined. The voltammetry of P_A is unusual for poly(RCOT)s in that it does not show an n-doping wave and also illustrates the history and relaxation effects common to other conjugated polymers. Electrochemical quartz crystal microbalance studies demonstrate that the p-doping of P_A and the n-doping of P_C proceed with the loss of ions and the formation of the internally compensated state.

The inability of large ions to diffuse through the polymer structure enables control over reactions between polymer films with different doping profiles and the means for fabricating such interfaces. A polyanion supporting electrolyte enables the selective oxidation ($P \rightarrow P^+$) of undoped P_A over P_C in a bilayer film using electrode potential ranges spanning $E^{\circ\prime}(P^+/P)$ for both P_C and P_A. The selective oxidation is realized through kinetic control over the ions available for charge compensation and requires the use of both appropriately functionalized conjugated polymers and a supporting electrolyte containing a polyion of the appropriate charge. The fabrication of the p-doped P_A | undoped P_C structure also illustrates the utility of using internal compensation as a means of inhibiting reactions between polymers with dissimilar doping profiles. Unlike traditionally doped conjugated polymers, internally compensated forms require an external source of mobile ions to support redox chemistry. When there is no such source, they are rendered kinetically stable toward reactions with a contacting phase.

Beyond enabling selective oxidation, polyanion supporting electrolytes are also useful in controlling other oxidative processes. In Bu_4NPSS, the electrochemistry of P_A is self-limiting. This permits the extent of oxidation to be controlled as much by polymer structure as it is by electrode potential. The density of ionic functionalities determines the ultimate level of oxidative doping possible, and this density is sufficiently low for P_A that it inhibits deleterious overoxidation effects that would otherwise occur at large positive potentials. The polyanion supporting electrolyte Bu_4NPSS also inhibits the reoxidation of n-type P_C to its undoped state by controlling the availability of the anions needed to support this process, thereby allowing the n-type polymer to be driven to relatively oxidizing potentials without complete loss of conductivity.

The control over electrochemical doping afforded by the use of a *combination* of conjugated ionomers and a polyion

(66) Shinohara, H.; Aizawa, M.; Shirakawa, H. *J. Chem. Soc., Chem. Commun.* **1986**, 87−88.
(67) Shimidzu, T.; Ohtani, A.; Iyoda, T.; Honda, K. *J. Electroanal. Chem.* **1987**, *224*, 123−135.

supporting electrolyte provides important tools for the fabrication of conjugated polymer structures incorporating regions of different doping type or density. Such structures are expected to exhibit interesting nonlinear and asymmetric current−voltage characteristics as is currently being explored.

Acknowledgment. This work was supported through the National Science Foundation CAREER Program (DMR-9703311), the Dreyfus New Faculty Program, the Beckman Young Investigator Program, and the University of Oregon. Partial support of the Center for Advanced Materials Characterization Laboratory (CAMCOR) at the University of Oregon was provided by the National Science Foundation (DMR-9601813) and the M. J. Murdock Charitable Trust.

JA016715Z